SUPPLEMENTARY MATERIAL

Materials and methods

Instrumentation and analytical techniques

We employed a NewWave UP193 Solid State Laser Ablation System (λ=193 nm) that was connected to a Thermo-Finnigan Element 2 sector field ICP-MS. Ablations used a pulse rate of 5 Hz, spot sizes between 50 and 75 µm, and irradiances between 0.16 and 0.24 GW/cm^2. Each measurement was preceded by a 40 s gas blank, and the transient signals of ^{11}B, ^{25}Mg, ^{27}Al, ^{43}Ca, ^{55}Mn, and ^{64}Zn were monitored. Al and Mn acted as indicators of sedimentary clay and ferro-manganese coatings, respectively. Zn was monitored in order to detect ablation of the sample holder consisting of a double-sided adhesive tape. Signals were calibrated using the NIST612 and 610 glasses (Pearce et al., 1997) that were measured between every five sample measurements. Calibration of many element/Ca ratios in carbonate samples with the NIST612 glass has been demonstrated to be accurate when using a 193 nm laser (Hathorne et al., 2008), but repeat analysis of a powder pellet of the CaCO$_3$ reference material JCt-1 (Okai et al., 2004) was performed to ensure accuracy and estimate analytical precision. Analysis of JCt-1 during this study produced an average B/Ca value of 172 µmol/mol, which is ~7% lower than the literature value (Okai et al., 2004). However, this number is within the external precision of ±10% (2σ) so we did not correct our data for this small offset. Based on 5 replicates, the external precision for B/Ca and Mg/Ca was calculated to ±10% and ±6% (2σ), respectively. Time resolved data were evaluated with the *GeoPro™* software (CETAC) using ^{43}Ca as internal standard.

The LA-ICP-MS technique provides information on the intra-shell heterogeneity of trace element/Ca ratios and is effective for analyzing B/Ca ratios in foraminifers, due to the low instrumental boron background. The limit of detection (LOD = 3 * SD$_{gas\ blank}$) for boron converted to concentration in the solid equals 4.5 ppm, at least a factor of 3 lower than the boron content of the analyzed foraminifera (~15 to 25 ppm). This background was found to be stable during the course of the multiple analytical sessions of this study in that the LOD did not change or the signal to background ratio remained >5.

Shells were not chemically or physically treated before analysis. Instead, ablation sites were pre-ablated for ~1 s in order to remove surface contamination. Only the umbilical sides of the shells, where pores are sparsely distributed, were analyzed to avoid the ablation of pore fillings. The time-resolved data of laser ablation measurements allows the distinction between shell calcite and potential contaminant phases such as secondary manganese-rich carbonate overgrowths that may affect bulk element/Ca ratios and are difficult to remove by chemical or physical cleaning. Following Boyle (1983), we excluded all phases with Mn/Ca ratios higher than 0.01 mmol/mol from the evaluation of core top data. For B/Ca measurements clay contamination is likely to be more problematic (Ni et al., 2007), so we have also excluded all data with Al/Ca ratios greater than 0.1 mmol/mol.

Core-top calibration

Foraminifer tests (size >250 µm, ~5 tests per sample) of *P. wuellerstorfi* (synonymous with *Cibicidoides or Fontbotia wuellerstorfi*) were picked from a total of 23 South Atlantic core top samples from different basins over a depth range from 1805 to 4675 m (Table DR1). Rose Bengal stained foraminifer shells show that individuals from surface sediment samples were recently living. Boron to calcium ratios were determined by analyzing each shell at five different spots (one in the center and four evenly spaced along the final whorl). Subsequently, mean values were averaged from ~25 spot measurements per sample. For core-top calibration of B/Ca against calcite saturation state (Δ[CO$_3^{2-}$]), modern seawater Δ[CO$_3^{2-}$] was calculated from WOCE data (WOCE Data Products Committee, 2002) using the eWOCE Electronic Atlas (Schlitzer, 2000) and the *CO2SYS* program (Pierrot et al., 2006). Carbonate system constants are from Mehrbach et al. (1973), refit by Dickson and Millero (1987), and the calcite saturation equation of Jansen et al. (2002).

***Reconstruction of Pleistocene* $\Delta[\text{CO}_3^{2-}]$**

For reconstructing Pleistocene $\Delta[\text{CO}_3^{2-}]$, a total of 29 samples spanning the last 135 k.y. were taken from three gravity cores retrieved in the equatorial Atlantic at 2945, 3984 and 4671 m water depths (Table DR2). Age models are based on graphic correlation of $\delta^{18}\text{O}$ records to the SPECMAP standard record (Imbrie et al., 1984). Calcite saturation state values were calculated from B/Ca ratios of *P. wuellerstorfi* using the linear regression derived from the core-top calibration (see previous section). The data are compared to the non-fragmented foraminiferal shell content in the same cores, which was determined by wet-sieving of bulk sediment over a 63 µm mesh sieve and weighing of dried samples (Bickert and Wefer, 1996). When foraminiferal shells are weakened by dissolution and break into smaller fragments, the material moves from the coarse fraction into finer fractions. The non-fragmented foraminiferal shell content is therefore sensitive to the carbonate corrosiveness of seawater and may thus be used as a quantitative proxy for the calcite saturation state (e.g., Wu and Berger, 1991). Peterson and Prell (1985) showed on a depth transect on the Ninetyeast Ridge that this proxy is much more sensitive to dissolution changes than the carbonate content because about 60% of the whole planktic foraminifer shells have already broken at the lysocline ($\Delta[\text{CO}_3^{2-}] \approx$ 20 µmol/kg), whereas no more than 20-30% of the carbonate have been lost. This is similar to our results showing that at $\Delta[\text{CO}_3^{2-}]$ between 50 and 0 µmol/kg the non-fragmented shell content decreased by ~40% while the carbonate content decreased by only ~20% (Fig. DR2). The fraction of non-fragmented foraminiferal shells, however, may also be subject to other processes such as the flux of foraminifer shells to the seafloor.

FIGURE DR1. Chamber-to-chamber variability of B/Ca and Mg/Ca in *P. wuellerstorfi*, where f is the final and f-1 the penultimate chamber, and so on. Error bars represent external precision (±2σ). Horizontal lines are the average values.
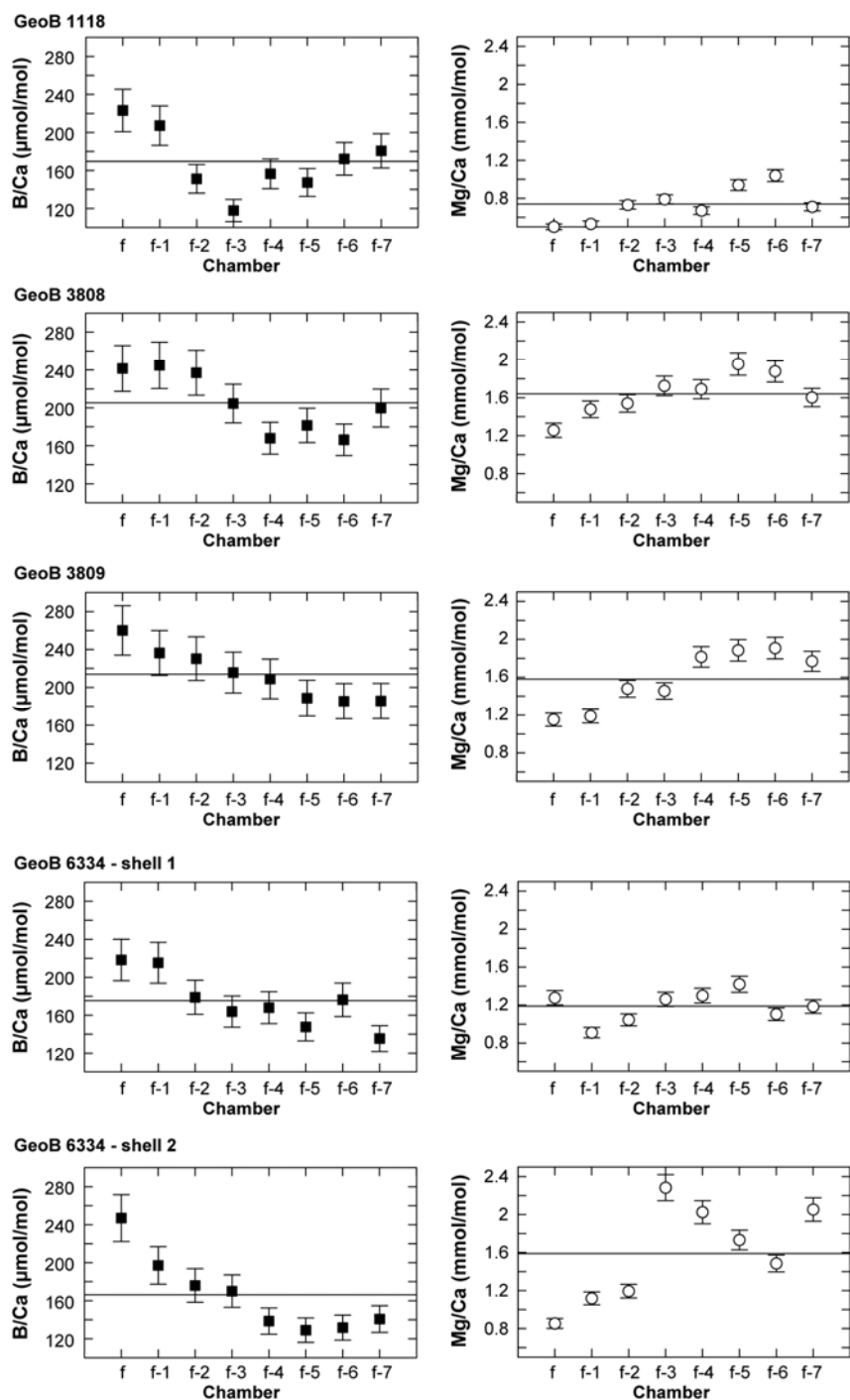
FIGURE DR2, Relationship between reconstructed $\Delta[CO_3^{2-}]$ (Table DR2) and the $CaCO_3$ content (left) and the non-fragmented foraminifer shell content (right) in the sediment. The non-fragmented shell content equates the grain size fraction >63 μm. Lines represent best non-linear fits through the data using a sigmoidal model. Both the carbonate content and the non-fragmented shell content are relatively insensitive at high $\Delta[CO_3^{2-}]$ because carbonate dissolution is negligible. At low $\Delta[CO_3^{2-}]$ the contribution of benthic foraminiferal shells to the non-fragmented shell content is relatively stable due to their low susceptibility to carbonate corrosivity of seawater, compared to planktic foraminifer shells.
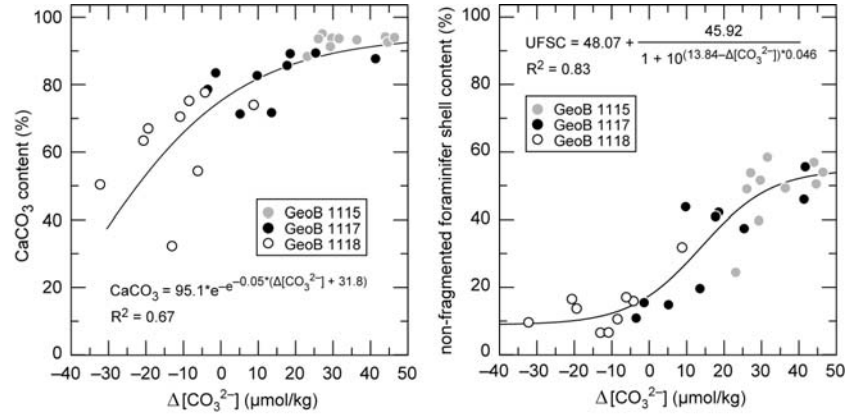
TABLE DR1. CORETOP SAMPLING LOCATIONS AND FORAMINIFERAL B/Ca RATIOS

GeoB Sample	Location Lat. °N	Long. °E	Water depth (m)	Temperature * (°C)	$\Delta[CO_3^{2-}]$ [†] (µmol/kg)	*P. wuellerstorfi* B/Ca ± SE (µmol/mol)
1041	-3.48	-7.59	4035	2.51	14.3	210 ± 7
1105	-1.67	-12.43	3231	2.36	30.5	216 ± 11
1118	-3.34	-16.26	4675	0.86	−14.9	166 ± 8
1710	-23.43	11.70	2987	2.57	27.3	226 ± 7
1715	-26.47	11.64	4095	1.43	3.0	191 ± 8
1720	-29.00	13.83	2011	2.95	38.1	208 ± 9
1721	-29.17	13.09	3045	2.43	24.6	186 ± 9
1728	-29.84	2.41	2887	2.35	28.2	229 ± 7
1729	-28.89	1.00	4401	2.36	5.2	211 ± 6
2102	-23.98	-41.20	1805	3.88	33.1	225 ± 13
2718	-47.31	-58.17	2991	1.20	13.7	180 ± 10
2727	-48.01	-56.54	2819	1.39	13.5	180 ± 12
3803	-30.35	-8.57	4173	2.43	10.6	199 ± 10
3804	-30.74	-8.77	3882	2.43	16.6	184 ± 10
3807	-30.75	-13.20	2515	2.51	34.0	226 ± 9
3808	-30.81	-14.71	3213	2.41	27.9	210 ± 7
3822	-27.63	-37.95	4273	0.43	−10.0	145 ± 11
3827	-25.03	-38.55	3842	1.53	11.8	176 ± 9
6208	-31.81	-45.67	3693	0.39	−1.6	159 ± 7
6222	-34.08	-48.62	3450	1.27	8.2	170 ± 10
6330	-46.15	-57.56	3874	0.43	−3.9	162 ± 7
6334	-46.09	-58.52	2597	1.57	20.3	172 ± 6
6336	-46.14	-57.84	3398	0.92	3.3	159 ± 9

* Bottom water temperatures derived from World Ocean Atlas WOA 2001 (Stephens et al., 2002)
[†] Calculated from WOCE data (WOCE Data Products Committee, 2002)
NOTE: Mg/Ca data from the same sample set is available in Raitzsch et al. (2008)

TABLE DR2. DOWNCORE SAMPLING LOCATIONS AND FORAMINIFERAL B/Ca RATIOS

GeoB core	Location Lat. °N	Long. °E	Water depth (m)	core interval (cm)	Age (ka)	*P. wuellerstorfi* B/Ca ± SE (µmol/mol)	Δ[CO$_3^{2-}$] * ± SE [†] (µmol/kg)
1115-3	–3.56	–12.56	2945	13-14	8	208 ± 6	27.1 ± 6.4
				63-64	19	221 ± 8	36.4 ± 7.4
				183-184	53	212 ± 7	29.7 ± 7.0
				213-214	65	203 ± 7	23.1 ± 7.1
				248-249	81	231 ± 7	44.0 ± 7.2
				268-267	87	232 ± 8	44.6 ± 7.6
				298-299	99	235 ± 7	46.4 ± 6.9
				328-329	110	211 ± 7	29.3 ± 7.2
				358-359	122	214 ± 10	31.6 ± 8.9
				683-684	135	207 ± 7	26.1 ± 7.2
1117-2	–3.81	–14.89	3984	23-24	8	228 ± 7	41.7 ± 7.2
				68-69	19	169 ± 8	–1.4 ± 7.4
				193-194	53	196 ± 12	18.5 ± 10.3
				233-234	64	178 ± 7	5.2 ± 7.9
				278-279	72	189 ± 7	13.6 ± 7.2
				298-299	87	206 ± 8	25.4 ± 7.4
				328-329	99	228 ± 10	41.3 ± 8.4
				358-359	110	195 ± 7	17.7 ± 6.9
				398-399	122	184 ± 6	9.7 ± 6.6
				433-434	135	166 ± 7	–3.5 ± 7.1
1118-3	–3.56	–16.42	4671	23-24	10	183 ± 6	8.8 ± 6.3
				53-54	20.9	159 ± 5	–8.5 ± 6.1
				158-159	55	165 ± 5	–4.2 ± 6.0
				188-189	63	127 ± 6	–32.3 ± 6.5
				203-204	71	153 ± 9	–13.1 ± 8.3
				218-219	81.8	162 ± 6	–6.2 ± 6.4
				233-234	87	145 ± 7	–19.4 ± 6.9
				318-319	122	143 ± 9	–20.7 ± 8.1
				348-349	135	156 ± 7	–10.9 ± 7.1

* Calculated using equation (1): $B/Ca = 1.37(\pm 0.23) * \Delta[CO_3^{2-}] + 170.9(\pm 4.8)$ (this study)
[†] propagated error from measurement precision of B/Ca and uncertainties of the regression (eq. 1)

References Cited

Bickert, T., and Wefer, G., 1996, Late Quaternary Deep Water Circulation in the South Atlantic: Reconstruction from Carbonate Dissolution and Benthic Stable Isotopes, *in* The South Atlantic: Present and Past Circulation, Berlin Heidelberg, Springer-Verlag, p. 599-620.

Boyle, E., 1983, Manganese carbonate overgrowths on foraminifera tests: Geochimica et Cosmochimica Acta, v. 47, no. 10, p. 1815-1819, doi:10.1016/0016-7037(83)90029-7.

Dickson, A., and Millero, F., 1987, A comparison of the equilibrium constants for the dissociation of carbonic acid in seawater media: Deep Sea Research Part A. Oceanographic Research Papers, v. 34, no. 10, p. 1733-1743, doi:10.1016/0198-0149(87)90021-5.

Hathorne, E., James, R., Savage, P., and Alard, O., 2008, Physical and chemical characteristics of particles produced by laser ablation of biogenic calcium carbonate: Journal of Analytical Atomic Spectrometry, v. 23, p. 240–243, doi:10.1039/b706727e.

Imbrie, J., Hays, J., Martinson, D., McIntyre, A., Mix, A., Morley, J., Pisias, N., Prell, W., and Shackleton, N., 1984, The orbital theory of Pleistocene climate: support from a revised chronology of the marine $\delta^{18}O$ record, *in* Milankovitch and Climate, Part I, Dordrecht, D. Reidel Publishing, 269 p.

Jansen, H., Zeebe, R.E., and Wolf-Gladrow, D.A., 2002, Modeling the dissolution of settling $CaCO_3$ in the ocean: Global Biogeochemical Cycles, v. 16, no. 2, doi:10.1029/2000GB001279.

Mehrbach, C., Culberso, C., Hawley, J., and Pytkowic, R., 1973, Measurement of apparent dissociation-constants of carbonic-acid in seawater at atmospheric-pressure: Limnology and Oceanography, v. 18, no. 6, p. 897-907, ISSN 0024-3590.

Ni, Y., Foster, G., Bailey, T., Elliott, T., Schmidt, D., Pearson, P., Haley, B., and Coath, C., 2007, A core top assessment of proxies for the ocean carbonate system in surface-dwelling foraminifers: Paleoceanography, v. 22, PA3212, doi:10.1029/2006PA001337.

Okai, T., Suzuki, A., Terashima, S., Inoue, M., Nohara, M., Kawahata, H., and Imai, N., 2004, Collaborative Analysis of GSJ/AIST Geochemical Reference Materials JCp-1 (Coral) and JCt-1 (Giant Clam): Chikyu Kagaku (Geochemistry), v. 38, no. 4, p. 281-286, ISSN 0386-4073.

Pearce, N., Perkins, W., Westgate, J., Gorton, M., Jackson, S., Neal, C., and Chenery, S., 1997, A compilation of new and published major and trace element data for NIST SRM 610 and NIST SRM 612 glass reference materials: Geostandards Newsletters, v. 21, no. 1, p. 115-144, doi:10.1111/j.1751-908X.1997.tb00538.x.

Peterson, L.C., and Prell, W.L., 1985, Carbonate dissolution in Recent sediments of the eastern equatorial Indian Ocean: Preservation patterns and carbonate loss above the lysocline: Marine Geology, v. 64, no. 3-4, p. 259-290, doi:16/0025-3227(85)90108-2.

Pierrot, D., Lewis, E., and Wallace, D. MS, 2006, Excel Program Developed for CO_2 System Calculations, ORNL/CDIAC-105: Carbon Dioxide Information Analysis Center, Oak Ridge National Laboratory, U.S. Department of Energy, Oak Ridge, Tennessee.

Raitzsch, M., Kuhnert, H., Groeneveld, J., and Bickert, T., 2008, Benthic foraminifer Mg/Ca anomalies in South Atlantic core top sediments and their implications for paleothermometry: Geochemistry Geophysics Geosystems, v. 9, no. 5, Q05010, doi:10.1029/2007GC001788.

Schlitzer, R., 2000, Electronic Atlas of WOCE Hydrographic and Tracer Data Now Available: EOS Trans. AGU, v. 81, no. 5, p. 45.

Stephens, C., Antonov, J., Boyer, T., Conkright, M., Locarnini, R., O'Brien, T., and Garcia, H., 2002, World Ocean Atlas 2001, vol. 1, Temperature, NOAA Atlas NESDIS 49: U.S. Govt. Print. Off., Washington, D. C.

WOCE Data Products Committee, 2002, WOCE Global Data, Version 3.0: WOCE International Project Office, Southampton, UK.

Wu, G., and Berger, W.H., 1991, Pleistocene $\delta^{18}O$ records from Ontong-Java Plateau: Effects of winnowing and dissolution: Marine Geology, v. 96, no. 3-4, p. 193-209, doi:16/0025-3227(91)90147-V.